Determination of Fracture Toughness Characteristics of Small-Size Chevron-Notched Specimens

Yevgeny Deryugin

Additional information is available at the end of the chapter

Abstract

A new method is proposed to determine fracture toughness of structural materials according to the test data of non-standard small-size chevron-notched specimens. During the tests, loading diagrams and photographic images of the specimens taken in time intervals are obtained. The crack length is measured in the process of its initiation and propagation. The analytical expressions are obtained being based and derived from the constitutive equations of engineering fracture mechanics to determine the crack-driving force (specific fracture energy) and the stress intensity factor. The method allows us to exclude the periodic unloading of the specimen applied under standard test conditions to determine the change in specimen compliance, which is taken into account in constitutive equations at crack length increase. All necessary calculation parameters are determined according to the experimental data. The method allows us to certify fracture toughness of the material without restrictions regarding the amount of plastic deformation and in front of the crack tip and in the specimen as a whole. The examples are given to calculate the fracture toughness criteria for a number of structural materials characterized by the ability to plastic deformation and by the Young's modulus value.

Keywords: fracture toughness, non-standard small-size chevron-notched specimens, analytical expressions, specific fracture energy, stress intensity factor, compliance

1. Introduction

Various methods for determining fracture toughness of materials are well-known and widely used when testing standard specimens with induced fatigue crack [1–3], when testing the Charpy notched specimens for fracture toughness [4], by the micro indentation method [5–7], et al.

An essential feature of these methods is that the characteristics of loading diagrams and the existing fracture length are measured, and then fracture toughness characteristics of the material are calculated by the semi-empirical formulas. As a rule, the critical stress intensity factor

(SIF) of the 1st kind K_{Ic} (for cleavage crack) is taken for the main fracture toughness characteristics of the material. The plane strain state condition of the loaded specimen is required in the experiments. In this regard, standard tests are conducted on specimens at least 10 mm thick.

Disadvantages of used methods are as follows:

1. There is no possibility to assess the fracture toughness of the material when testing the small thickness specimens;

2. Complexity of the mechanical processing and manufacturing of specimens;

3. Requirement for the fatigue pre-cracking on the notch;

4. Availability of special test equipment;

5. Use of significant amount of the complex-shaped specimens (cut out by layers, holes, notches);

6. Need for the high power load device;

7. High steel intensity of test specimens.

8. Need for periodic unloading of the specimen to determine the change in specimen compliance under loading.

9. Availability of phenomenological constants in constitutive equations, taking into account the geometric shape and boundary loading conditions.

As a rule, during a fracture toughness test of small-size specimens, the chevron-notched specimens are used [7–11]. The specimens with this configuration do not require the preliminary fatigue crack. When testing the small-size chevron-notched specimens, many of the above-mentioned problems are absent.

This chapter proposes a new method for fracture toughness determination of structural materials using the small-size chevron-notched specimens. The method allows us to determine fracture toughness characteristics without severe restrictions on the specimen ability to plastic deformation. There are no phenomenological dependencies and empirical constants in the calculations.

The fracture toughness characteristics comply with the conditions of continuous loading of specimens, without using the "loading-unloading" operation.

The important calculation works were carried out associated with the use of chevron-notched specimens during testing.

2. Fracture toughness calculation of straight-through notched specimens

To determine the global failure conditions, irrespective of the material state and geometrical dimensions of the specimen, the energy approach is appropriate [12]. The key point of the energy fracture criterion in fracture mechanics is formulated as follows: the crack growth can

occur if the system can release energy required to initiate crack propagation to the elementary distance dl. The energy needed for crack growth, appears only due to the elastic deformation energy that occurs in-side the material under the applied external force.

The reliable fracture toughness characteristic is the critical value of the elastic energy release rate (ERR) during the crack propagation G_c. In the two-dimensional version, this characteristic is equivalent to the value of the J-integral [13, 14]. For brevity, the value of G will be called specific fracture energy. The specific fracture energy (SFE) is defined as energy that is spent on the formation of the crack surface with area 1 m^2. The unit of measurement for SFE is J/m^2.

In practice, there is a decrease in specimen stiffness or structure at initiation and propagation of the crack. The specimen stiffness M is defined as the ratio of load P, applied to the specimen, to the displacement of load application point λ_e at elastic deformation of the specimen: M = P/λ_e.

The reciprocal of the stiffness is defined as a specimen compliance η: $\eta = \lambda_e/P$.

The necessary condition for through-crack propagation in the flat specimen of unit thickness obeys the equation [12–14]

$$G = \frac{P^2 d\eta}{2dl},$$ (1)

where $d\eta/dl$ is the change in specimen ductility during crack propagation, dl is the short distance, to which a straight-line crack front propagates. At the stage of stable crack propagation, this value characterizes the fracture toughness G_c of the material. As follows from Eq. (1), elastic energy per unit of new crack surface at its propagation to dl in the specimen in thickness a is equal to

$$G = \frac{P^2 d\eta}{2adl} = \frac{P^2 d\eta}{dS},$$ (2)

where $dS = 2adl$ is the elementary increment of the crack surface area.

There is a classic example for calculating the stress intensity factor K_I to test a double cantilever beam specimen with a straight-through notch [15]. The relation between G and K_I for the plane stress state obeys the equation

$$G = K_I^2 (1 - v^2)/E.$$ (3)

Let us consider the case of double-cantilever beam specimens with a straight-through notch in detail, since the result will be used in the calculation of G for the chevron-notched specimens.

Figure 1 presents the double-cantilever beam specimens with a straight-through notch. Distance from the load application point P to the crack front is the initial crack length l. As follows from the cantilever bending theory, displacement of the load application point λ_e (**Figure 1**) is equal to $\lambda_e = \frac{4P}{Ea}\left(\frac{l}{b}\right)^3$, where E is the Young's modulus, b is the cantilever thickness. For the double cantilever beam specimen, displacement of load application points ζ is $2\lambda_e$. Therefore, the specimen ductility η is $\eta = \frac{\zeta}{P} = \frac{8}{Ea}\left(\frac{l}{b}\right)^3$.
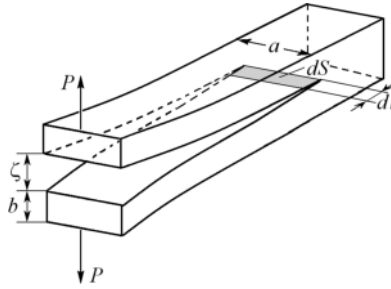
Figure 1. Straight-through-notched specimen.

The ductility derivative by the crack length is equal to

$$\frac{d\eta}{dl} = \frac{24l^2}{Eab^3}. \tag{4}$$

Substitution of Eq. (4) into Eq. (1) leads to the following expression for SFE [13, 15]

$$G = \frac{12P^2l^2}{Eb^3a^2}. \tag{5}$$

According to Ref. [14], the displacement λ_e of the cantilever end under elastic deformation for the specimen in thickness of a with a crack length l is provided by the load:

$$P = \frac{E\lambda_e a}{4}\left(\frac{b}{l}\right)^3. \tag{5a}$$

Substituting this expression into Eq. (4), we obtain the equation for G that allows us to calculate fracture energy by the crack length l and by the elastic opening value of the notch tips λ_e [16]:

$$G = \frac{3\lambda_e^2 b^3 E}{4l^4}. \tag{6}$$

In the given representation, the value of G does not depend on the specimen thickness a.

Eq. (5) determines SFE by the crack length l, and by the external load value P, at which spontaneous crack propagation begins. Basically, SFE can be calculated according to Eq. (6) when testing the small-size specimens. It should be noted that there are no any empirical constants in Eq. (6). All necessary values can be taken from the experiment. To maintain the experimental integrity, one can grow a fatigue crack at the tip of the notch. However, this method has several disadvantages.

Eq. (5) gives only a rough approximation of the SFE value. There is a certain divergence due to the fact that the cantilevers' ends are fixed not absolutely rigidly, as in the cantilever embedded in the rigid base. But this is not the most important thing. The main disadvantage is that in practice crack propagation along the notch plane is not guaranteed. Consequently, deviations in crack propagation direction cause shear deformations. Besides, crack front straightness is not preserved. To some extent, this problem is solved by using the chevron-notched specimens.

3. Fracture toughness calculation of the chevron-notched specimens

When testing the small-size specimens, generally, the chevron-notched specimens are used [7, 17]. For the first time, a chevron-notched specimen was proposed by L.M. Barker in 1977 to determine fracture toughness under plane strain conditions [17].

Standard tests of the chevron-notched specimen are conducted according to the scheme presented in **Figure 2**.

Figure 3 shows examples of the chevron-notched specimens. The specimens of this configuration do not require the preliminary guidance of a fatigue crack to the tip of the notch. From the moment of loading, there is a high stress concentration at the tip of the chevron notch that is sufficient to crack initiation. It is assumed that the development of plastic deformation in the chevron zone satisfies the plane strain state condition. The crack initiated at the tip of the chevron, can propagate only along the notch plane. At the same time, there is a high probability that the crack front during propagation, at the average, maintains a straight shape. The chevron notch geometry allows us to fix and extend the stable crack propagation stage and, thus, to calculate the beginning of the specimen catastrophic failure more accurately.

As a rule, short circular specimens are used in the experiments (**Figure 3a**). The disadvantage of the standard method for measuring fracture toughness of the chevron-notched specimens is that in order to determine the change in specimen ductility, the "loading-unloading" condition
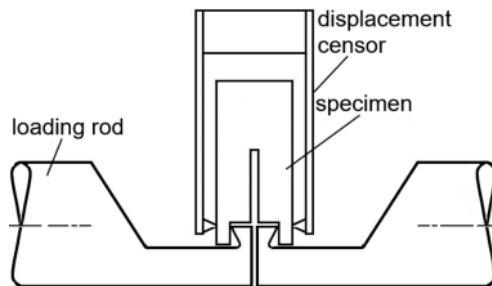

Figure 2. Loading configuration of the chevron-notched specimen.
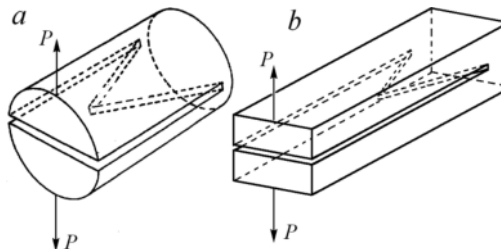

Figure 3. The chevron-notched specimens: short circular specimen (*a*) and elongated rectangular specimen (*b*).

should be carried out. For this reason, the calculation formulas include adjustable coefficients considering the non-linear behavior of the material and a complex geometric shape of the notch.

This section provides a new method for calculating the fracture toughness characteristics of materials when testing the chevron-notched specimens. The novelty is in the fact that the calculation of SFE is based on calculation of the energy and power parameters of the specimen taking into account the complex geometry of a chevron notch according to the strict laws of solid mechanics. It is convenient to make calculations and experiments for the elongated rectangular specimen (**Figure 3b**). In this case, the chevron-notched specimen has a shape of a double cantilever beam configuration.

Let us determine the relation of the external force P with an elastic deflection λ_e of the single cantilever of the specimen. The cantilever can be represented as a set of elementary cantilevers (minicantilevers) of the infinitely small width dx. **Figure 4** shows the projections of the chevron-notched specimens. The minicantilever length at a distance x from the symmetry axis of the specimen is $l(x) = l_0 + x \cdot \text{ctg}(\alpha/2)$, where l_0 is the minimum distance from the load application point to the chevron notch, α is the chevron angle (**Figure 4**). For each minicantilever in the set, the well-known elasticity theory formula is valid [14]:

$$\lambda_e = \frac{4dP(x)}{Edx}\left(\frac{l(x)}{b}\right)^3, \tag{7}$$

where λ_e is the elastic deflection of the minicantilever, dP is the elementary load, under the action of which the cantilever in thickness of dx is deflected to the value of λ_e, b is the thickness of the minicantilever. In view of this, from Eq. (6) we obtain the elementary load dependence dP, applied to the end of the minicantilever on its width dx:

$$dP(x) = \frac{\lambda_e E}{4}\left(\frac{b}{l(x)}\right)^3 dx. \tag{8}$$

Integration of elementary forces (7), affecting each minicantilever across the specimen width a, will clearly determine the actual load P, providing the minicantilever's deflection by λ_e:

$$P = \frac{\lambda_e b^3 E}{4}\int_{-\frac{a}{2}}^{\frac{a}{2}} dx \Big/ \left(l_0 + x \cdot \text{ctg}\,\frac{\alpha}{2}\right)^3, \text{ or } P = \frac{E\lambda_e a}{4}\left(\frac{b}{l_0}\right)^3\left[4 + \frac{a}{l_0}\,\text{ctg}\,\frac{\alpha}{2}\right]\Big/\left[2 + \frac{a}{l_0}\,\text{ctg}\,\frac{\alpha}{2}\right]^2 = \frac{E\lambda_e a}{4}\left(\frac{b}{l_0}\right)^3 k' \tag{9}$$

This equation differs from Eq. (5) from the straight-through notch only by the factor

$$k' = l_0[4l_0 + a\,\text{ctg}\,(\alpha/2)][2l_0 + a\text{ctg}\alpha/2]^{-2}. \tag{10}$$

According to Eq. (9), a single cantilever elastic deflection of a double cantilever beam specimen with a chevron notch is $\lambda_e(l_0) = \frac{4P}{Ea}\left(\frac{l_0}{b}\right)^3 k'^{-1}$.

During the loading, the moment of crack initiation occurs at the tip of the chevron notch. Propagation of the initiated crack to the distance Δl increases the effective fracture length. Let us present the crack front as a straight line (**Figure 5**). The length of this line is $h = 2\Delta l \cdot \text{tg}(\alpha/2)$.
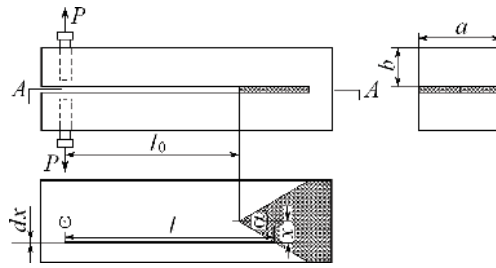
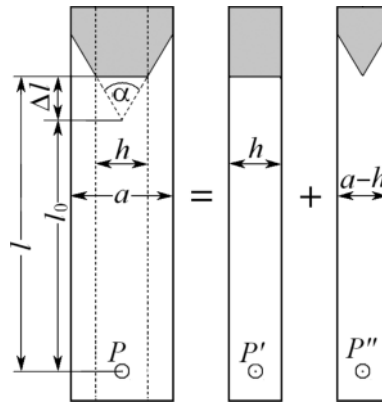**Figure 4.** Projections of chevron-notched specimen.

Figure 5. Presentation of the specimen with a crack in the form of straight-through and chevron-notched specimens.

Basically, this specimen with a crack is a set of two specimens: with a straight-through notch in width of h and with a chevron notch in width of $a - h$ (**Figure 5**). Let us determine the forces P' and P'' for these specimens, respectively, causing identical deflection λ_e. Using Eq. (5), we find an expression for P' acting on a straight-through notched specimen in width of $h = 2\Delta l \cdot \text{tg}(\alpha/2)$:

$$P' = \frac{\lambda_e E \Delta l}{4} \, \text{tg} \, \frac{\alpha}{2} \left(\frac{b}{l}\right)^3. \tag{11}$$

According to Eq. (9), for the chevron-notched specimen in width of $a - h$, we obtain an expression for P'':

$$P'' = \frac{\lambda_e \Delta l \cdot \text{tg} \, \frac{\alpha}{2} E}{4} \left(\frac{b}{l}\right)^3 \left(1 - \frac{2\Delta l}{a} \, \text{tg} \, \frac{\alpha}{2}\right) \frac{l}{l_0} \left[4 + \frac{a}{l_0} \, \text{ctg} \, \frac{\alpha}{2} + \frac{2\Delta l}{l_0}\right] \Big/ \left[2 + \frac{a}{l_0} \, \text{ctg} \, \frac{\alpha}{2}\right]^2. \tag{12}$$

On the basis of Eqs. (11) and (12), an expression for λ_e is determined:

$$\lambda_e(l) = \frac{4P}{Ea} \left(\frac{l}{b}\right)^3 k^{-1}, \tag{13}$$

where $P = P' + P''$, $l = l_0 + \Delta l$ and k is

$$k = \frac{2\Delta l}{a}\, \text{tg}\,\frac{\alpha}{2} + \frac{l}{l_0}\left(1 - \frac{2\Delta l}{a}\,\text{tg}\,\frac{\alpha}{2}\right)\left(4 + \frac{a}{l_0}\,\text{ctg}\,\frac{\alpha}{2} + \frac{2\Delta l}{l_0}\right)\left[2 + \frac{a}{l_0}\,\text{ctg}\,\frac{\alpha}{2}\right]^{-2}.$$

It is easy to verify that at $\Delta l \rightarrow 0$, the value of $k \rightarrow k'$.

Substituting Eq. (13) for λ_e into Eq. (6), we obtain the expression for SFE:

$$G = \frac{12P^2 l^2}{Eb^3 a^2}k^{-2}. \tag{14}$$

This equation differs from the similar one for the straight-through notch only by k^{-2}. In particular, if $\alpha = \pi$, Eq. (14) goes over into Eq. (5) for the straight-through notch, since then k is 1.

As follows from Eq. (14), the characteristic of G depends on the Young's modulus E. The higher E is, the lower is the SFE value under all other conditions being equal. In contrast, according to Eq. (2), characteristic of K_I does not depend on E, i.e. SIF is invariant in relation to the Young's modulus.

4. Theoretical determination of elastic crack opening δ_e

The specimen presentation in the form of a double cantilever configuration allows us to determine the elastic crack opening initiated at the tip of the chevron. It is known that the elastic displacements of the cantilever points obey equation [14]:

$$v_e(x) = \frac{P}{Ea}\left[2\left(\frac{x}{b}\right)^3 - 6\frac{x}{b}\left(\frac{l}{b}\right)^2 + 4\left(\frac{l}{b}\right)^3\right], \tag{15}$$

where the x axis is directed along the cantilever. At $x = 0$, Eq. (15) determines the elastic deflection λ_e of the load application point P.

Eq. (15) is also valid for the double cantilever beam specimen with a straight-through notch. Then elastic notch opening in the point x is $\delta_e(x) = 2v_e(x)$. The cantilever displacement in the point $x = l_0$ is equal to

$$v_e(l_0) = \frac{2Pl_0\Delta l^2}{Eab^3}\left[3 + 2\frac{\Delta l}{l_0}\right]. \tag{16}$$

Substituting Eq. (5a) for P into Eq. (16), we obtain the cantilever displacement in the point $x = l_0$ for the straight-through notched specimen:

$$v_e = \lambda_e \frac{\Delta l^2[3l_0 + 2\Delta l]}{2(l_0 + \Delta l)^3}. \tag{17}$$

Let us find the cantilever displacement in the point $x = l_0$ for the chevron-notched specimen. For this, we use Eq. (16), where we place the value of P' instead of P according to Eq. (11), and

the width of the specimen central part $h = 2\Delta l \cdot \text{tg}(\alpha/2)$ shown in **Figure 5** instead of a. Let us find the cantilever deflection in the load application point P':

$$\lambda_e = \frac{2P'}{E\Delta l \cdot \text{tg}(\alpha/2)}\left(\frac{l_0 + \Delta l}{b}\right)^3. \tag{18}$$

Alternately, as follows from Eq. (17),

$$\lambda_e = \frac{\upsilon_e 2(l_0 + \Delta l)^3}{(3l_0 + 2\Delta l)\Delta l^2}. \tag{19}$$

From Eqs. (18) and (19), we obtain an expression for P':

$$P' = \frac{\upsilon_e E b^3 \text{tg}(\alpha/2)}{(3l_0 + 2\Delta l)\Delta l}. \tag{20}$$

As follows from Eq. (12), $\lambda_e = \frac{4l^2 \cdot \text{ctg}(\alpha/2)(P - P')}{Eb^3[a - 2\Delta l \, \text{tg}(\alpha/2)]} \frac{[2l_0 + a \, \text{ctg}(\alpha/2)]^2}{[4l_0 + a \text{ctg}\alpha/2 + 2\Delta l]}$.

Taking into account Eq. (20), we find a cantilever point displacement at a distance l_0 from the load application point P:

$$\upsilon_e = \frac{P(l_0 + 2l)\Delta l}{Eb^3 \text{tg}(\alpha/2)} - \frac{\lambda_e \Delta l(l_0 + 2l)[a - 2\Delta l \, \text{tg}(\alpha/2)][4l_0 + a \, \text{ctg}(\alpha/2) + 2\Delta l]}{4l^2 \text{tg}(\alpha/2)[2l_0 + a \, \text{ctg}(\alpha/2)]^2}. \tag{21}$$

The value of $\delta_e(l_0) = 2\upsilon_e$ determines the crack opening initiated at the chevron.

During the crack propagation, the increment of the single cantilever elastic deflection occurs in the load application point P. The increment

$$\Delta\lambda_e = \lambda_e(l_0 + \Delta l) - \lambda_e(l_0), \tag{22}$$

corresponds to the crack length Δl.

Figure 6 presents the curves of the υ_e dependence on the crack length Δl and on the increment of the single cantilever elastic deflection $\Delta\lambda_e$ obtained using Eq. (21), at following values of the parameters: $E = 110$ GPa, $l_0 = 18.12$ mm, $\Delta l = 3.77$ mm, $P = 822$ H, $\alpha = \pi/9$ (20°), $a = b = 4.35$ mm. The calculations show that there is a parabolic dependence between Δl and υ_e, which can be written as $\upsilon_e = A\Delta l^2$, where A is the constant, which depends on the assignment of concrete parametric values in Eq. (21). In this case, A is equal to 2.58. As seen from the plot, there is a linear dependence $\Delta\lambda_e = B\upsilon_e$ between $\Delta\lambda_e$ and υ_e. The proportionality factor for the assigned values of B is 5.969.

The equations given above are derived from the constitutive equations of engineering fracture mechanics for the first time and can be used for the calculation of SFE for the chevron-notched specimens.

The processes of plastic deformation affect the cantilever deflection value and opening of crack sides in the point of its initiation. For this reason, the experimentally measured values of the
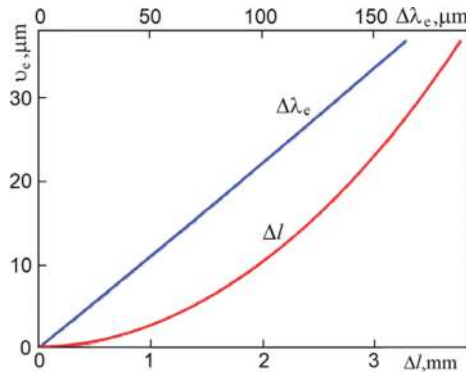
Figure 6. Dependence υ_e on Δl and $\Delta\lambda_e$.

cantilever deflection λ, except for λ_e, contain a part of the equation $\lambda_p = \lambda - \lambda_e$ that is not related to the change in specimen ductility. The crack opening values of υ measured in the same way contain the plastic deformation contribution $\upsilon_p = \upsilon - \upsilon_e$. The values of λ_p and υ_p are very important when simulating the fracture process in the chevron-notched zone.

Using Eq. (13), according to the experimentally measured value of cantilever deflection λ (**Figure 7**), one can determine the relative value of $(\lambda-\lambda_e)/\lambda_e = \lambda_p/\lambda_e$ as an additional fracture toughness characteristic. It is obvious that the more ductile a material is, the higher is its fracture toughness. The value of λ_p is not associated with change in specimen ductility since it is determined only by the elastic deflection of the specimen. The stress distribution in the plastic deformation zone is significantly different from the stress field in an elastic medium with a crack. On the way of crack propagation, the material is always subjected to a certain degree of plastic deformation. This means that crack is always surrounded by a layer of the plastically deformed material. The calculations made in Ref. [21] by the method of relaxation elements showed that stress field in the plastic deformation zone differs significantly from the crack stress field in the elastically deformable medium. Plastic deformation leads to stress relaxation. For this reason, there is no singularity in the crack mouth. The maximum stress concentration is observed in the plastic deformation zone.
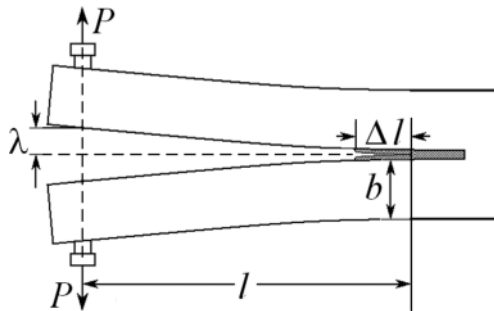

Figure 7. Scheme of the cantilever deflection.

The above equations are derived without any assumptions about the plastic properties of the material. Therefore, they can be used to calculate fracture toughness of any structural materials wherein the crack initiation at the tip of the chevron notch is observed. The product of $EG/(1 - \nu^2)$ does not depend on the Young's modulus since SFE G is inversely proportional to the Young's modulus value E (see Eq. (14)). Therefore, irrespective of plastic properties of the material, the equation

$$K_I = \sqrt{\frac{EG}{(1 - \nu^2)}} = \frac{2Pl}{ab^{3/2}k}\sqrt{\frac{3}{1 - \nu^2}} \qquad (23)$$

determines the stress intensity factor (SIF) for the small-size chevron-notched specimens.

The standard test on ductility change of the chevron-notched specimens is made using the "loading-unloading" operations [7, 8, 18–20]. As a result, the fracture toughness of the material is determined under the low-cycle loading conditions, rather than under constant loading. It is known that the curve type "load-displacement" changes significantly depending on the previous loading history. This is due to the fact that the plastic deformation rate and strain hardening of the material essentially depend on the external load and time during which the load is acting. To define the mechanisms of failure of structural materials, first of all, the values of SFE and SIF under continuous loading are significant. Eqs. (13) and (15) allow us to calculate these characteristics with-out using the load-unload condition. It is enough to know the crack length Δl initiated at the chevron.

The examples of the fracture toughness analysis of a number of structural materials, which differ in their ability to crack formation and the Young's modulus, are presented below.

5. Fracture toughness of structural materials

This section presents the calculation results of the fracture toughness characteristics of VT6 (Ti + 6%Al + 4%V) alloy, Fe-35.4% Ni and 12GBA tube steel.

The specimens $21 \times 10 \times 6 \ mm^3$ in size were cut from the work piece by the electroerosion method. Then a notch 0.3 mm thick was made with a chevron angle $\alpha = 60°$ (see **Figure 4**). The crack length at the pre-fracture stage was determined by the specimen images. Alloys with different ability to plastic deformation and with different values of the Young's modulus E were tested. The loading of specimens made of VT6 and Fe + 34.6%Ni alloys was performed by the intrusion of a narrow wedge into the notch at a motion rate of 5 μm/s (**Figure 8**). The 12GBA tube steel loadings were performed by application of opposite forces to the tips of the notch (**Figure 7**).

Figure 8 shows the scheme of the specimen wedging. The constant motion rate of the wedge provides the prolonged stage of stable crack propagation initiated at the chevron. The equation for the calculation of P bending the cantilever is obtained from the condition of equilibrium of forces:

$$P = \frac{F \cdot \cos\gamma}{2\left[\sin\left(\beta/2\right) + \kappa \cdot \cos\left(\beta/2\right)\right]}, \tag{24}$$

where F is the load on the wedge, κ and γ are the friction factor and interplanar angle between the wedge and cantilever, respectively, β is the angle of wedge opening.

As seen from Eq. (19), in order to determine the bending force P, it is important to calculate the friction factor κ. Substituting Eq. (22) into Eq. (8) instead of P, we obtain the following equation for κ:

$$\kappa = \frac{\Delta F}{\Delta L} \frac{2\cos\gamma\left[2l_0 + a\,\text{ctg}\left(\alpha/2\right)\right]^2}{\sin\left(\beta/2\right)\left(4l_0 + a\,\text{ctg}\left(\alpha/2\right)\right)aEl_0} \left(\frac{b}{l_0}\right)^3 - \text{tg}\,\frac{\beta}{2}, \tag{25}$$

where $\Delta F/\Delta L$ is the decline of the initial elastic segment of the experimental loading diagram "load P–wedge displacement L".

The calculations showed that κ is equal to 0.08 to an accuracy of 10%.

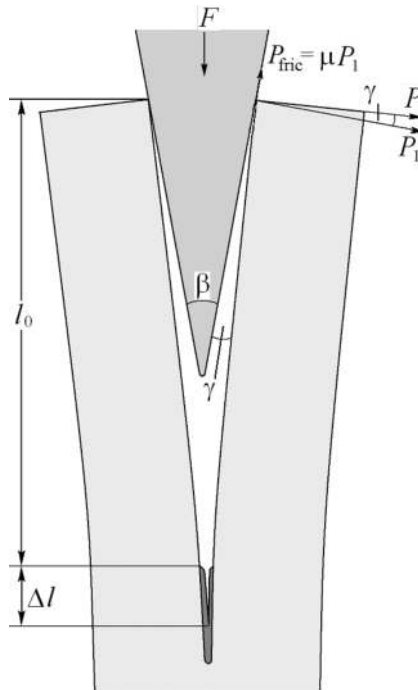**Table 1** shows the fracture toughness characteristics of the studied materials.

Figure 8. The scheme of the chevron-notched specimen wedging.

Alloy	P, N	λ_e, mm	λ, mm	λ_p/λ_e	υ_e, μm	υ, μm	υ_p/υ_e	G, kJ/m^2	K_I, MPa·m$^{1/2}$
VT6 UFG	277.7 (max)	0.453	0.453	0	0	0	–	11.9	35.5
	193.1 (stable)	0.407	0.374	0.09	15.1	23.8	0.53	4.58	22.5
VT6 CC	522.6 ($\Delta l = 0$)	0.827	1.275	0.54	0	0	–	43.04	68.81
	584.1 (max)	1.162	2.100	0.81	39.6	162.5	3.10	43.40	69.09
Ni-Fe	936.0 ($\Delta l = 0$)	0.426	0.474	0.11	0	0	–	23.63	70.44
	1175.2 (max)	0.695	1.038	0.49	30.8	89.9	1.92	30.27	75.51
12GBA	2776 (max)	0.095	0.379	2.6	0	0	–	51.7	104.2

Table 1. Fracture toughness characteristics of structural materials.

5.1. VT6 alloy (Ti–6Al–4V)

The structural VT6 alloy is mainly used for the manufacturing of large welded and built-up air-craft structures, balloons working under internal pressure over a wide temperature range from 196 to 450°C, and a number of other structural elements.

The studies were conducted using the material in the initial coarse-crystalline (CC) state (grain size of 7–5 μm) and with ultra-fine grained (UFG) structure (grain size of 500 nm) obtained by the severe plastic deformation [22]. The loading was carried out by a wedge with β equal 20° (**Figure 8**).

Figure 9 shows a typical loading diagram of the UFG VT6 alloy. The load-peak corresponds to the moment of crack initiation at the tip of the chevron. A sudden stress drop is caused by the spontaneous crack propagation to a certain length along the chevron notch. After that there is slow and stable crack propagation to the critical length, which determines the final fracture of the material. In the calculations for the VT6 alloy, E was equal to 110 GPa [23–25].

The measured values of l_0 and Δl are equal to 18.12 and 3.767 mm, respectively, $a = b = 4.35$ mm. The same values were used for calculating the fracture toughness of the VT6 alloy in the coarse-crystalline state (CC).
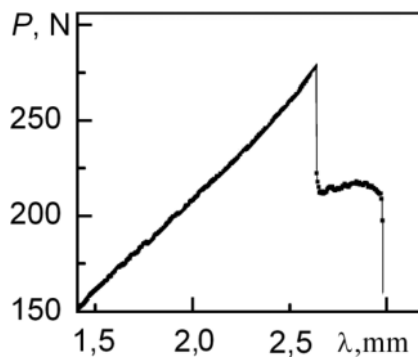

Figure 9. Loading diagram of UFG VT6 alloy.

Table 1 shows that plastic deformation does not affect the displacement of the notch sides prior to the crack initiation in the UFG VT6 alloy ($\lambda_p/\lambda_e = 0$). This means that the specimen is deformed only elastically prior to crack initiation. At the stage of pre-fracture, the influence of plastic deformation was observed: $\lambda_p/\lambda_e = 0.09$. The contribution of plastic deformation to the crack opening at the tip of the chevron is comparable with that of elastic deformation: $\upsilon_p/\upsilon_e = 0.53$.

Spontaneous crack propagation from the moment of its initiation is accompanied by the reduction in the elastic deflection λ_e of a single cantilever of the specimen and reduction in the fracture tough-ness characteristics of G and K_I. This alloy shows quite different fracture regularities in the coarse-crystalline state. A qualitative view of the loading diagrams and consistent patterns of crack propagation in the chevron-notch zone (**Figure 10**) show the following. The beginning of crack initiation and propagation occurs long before the external load reaches a maximum. This is marked with an arrow 1 shown in **Figure 10**. Crack initiation is preceded by the plastic deformation of the material in the chevron-notch zone. The contribution of plastic deformation λ_p to the displacement of load application point P up to the moment of crack initiation is comparable with that of elastic deformation: $\lambda_p/\lambda_e = 0.54$ (see **Table 1**).

Peaks and plateaus on the loading diagram are caused by abrupt nature of crack propagation. The specific fracture energy of G and K_I is almost unchanged until it reaches the maximum load P_{max} marked with an arrow 2 in **Figure 10**. Thus, a fracture toughness criterion for the CC VT6 alloy are the values of SFE $G_c = 43.2 \pm 0.2$ kJ/m^2 and SIF $K_{Ic} = 68.9 \pm 0.2$ MPa·m$^{1/2}$. The SIF value coincides with the value of 66.4 MPa·m$^{1/2}$ to an accuracy of 3.6% in Ref. [24] for standard test conditions.

During crack propagation, a contribution of plastic deformation to the displacement of the notch tips increases. The equation $\lambda_p/\lambda_e = 0.81$ corresponds to the maximum load. The contribution of plastic deformation to the crack opening at the tip of the chevron is 3 times higher than that of elastic deformation: $\upsilon_p/\upsilon_e = 3.1$. The subsequent loading leads to a drop in the external load and to the reduction of G and K_I characteristics. In this case, the λ_p/λ_e ratio goes up due to the λ_p increase and λ_e decrease.
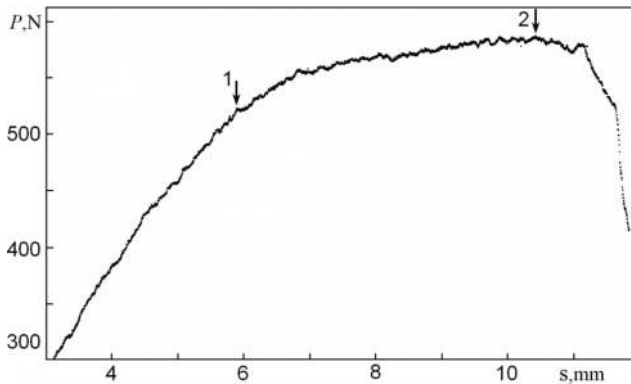

Figure 10. Loading diagram of the CC VT6 alloy.

A comparison shows that the method used to obtain the UFG structure in the VT6 alloy leads to a strong decrease in ductility, crack initiation stress (two-fold) and stress of stable crack propagation (three-fold). For this reason, the SMC VT6 alloy is characterized by the low fracture toughness. The behavior of the SMC VT6 alloy can be explained as follows. The low ductility of the alloy practically eliminates the stress relaxation factor in the chevron-notch zone and, as a consequence, reduces the crack initiation stress in the chevron. Stable propagation is determined by the stress con-centration at the tip of the crack, which is higher than that at the tip of the chevron prior to crack initiation. In this connection, a stress decrease takes place. The calculations have shown that the fracture toughness criteria for the SMC VT6 alloy are the values of SFE $G_c = 4.58 \pm 0.2$ kJ/m^2 and SIF $K_{Ic} = 22.5 \pm 0.2$ MPa·m$^{1/2}$ at the stage of stable crack propagation.

5.2. The Fe + 34.6%Ni-alloy

Table 1 also includes the data for the iron-nickel invar Fe + 34.6% Ni, which is widely used in modern industry and technology as an alloy with thermal linear expansion coefficient (TLEC) close to zero. When loading the specimen, a wedge with $\beta = 40°$ was used.

The structural state of the alloy corresponds to that after the multi-axial forging. The alloy has a polycrystalline structure with an average crystallite size d equal 8 μm. The value of Young's modulus E in the calculation is 210 GPa. **Figure 11** shows a loading diagram of this alloy. The moment of crack initiation at the tip of the chevron is marked with an arrow 1. The beginning of crack initiation and propagation occurs long before the external load reaches a maximum. According to Eq. (13), the SFE from the moment of crack propagation (at $\Delta l = 0$) is equal to $G = 23.6 \pm 0.20$ kJ/m^2. The corresponding value of K_I is 70.5 ± 0.1 MPa·m$^{1/2}$.

The intermittent nature of the loading curve demonstrates that crack propagation occurs abruptly. Experimentally measured displacement of the load application point up to the moment of crack initiation is $\lambda = 0.47 \pm 0.02$ mm. According to Eq. (12), the portion of displacement that takes place due to the specimen elastic deformation is $\lambda_e = 0.43 \pm 0.02$ mm. Therefore, within the limits of the experimental error, the relative value of λ_p/λ_e does not exceed 10%. Thus, the plastic deformation prior to the moment of crack initiation in the chevron makes a minor contribution to the displacement of the load application point.
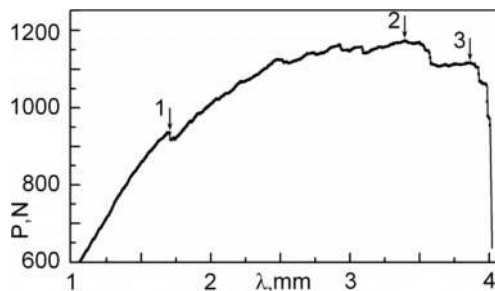

Figure 11. Loading diagram of the Fe-Ni alloy.

The observations show that the crack propagates along a complex trajectory, sharply changing the motion direction (**Figure 12**). The maximum value of SFE $G_c = 30.8 \pm 0.3$ kJ/m^2 corresponds to the maximum load. The corresponding value of K_{Ic} is equal to 80.4 ± 0.2 MPa·m$^{1/2}$. Note that the value obtained practically coincides with those of $K_c = 81.2$ MPa·m$^{1/2}$, obtained for the Fe-17%Ni alloy [26]. The critical value of crack opening $\delta_e = 2\upsilon_e = 61.56$ μm can also be used as a fracture toughness characteristic. The experimental value of δ is 179.8 μm. Hence, υ_p/υ_e is equal to 1.92. Thus, at the stage of prefracture, the crack opening in the chevron-notch zone contains a significant contribution related to the plastic deformation, which is almost twice greater than that of the elastic deformation of the specimen. A subsequent increase in crack length leads to a drop in the values of G_c and K_{Ic}. In this case, the υ_p/υ_e ratio increases due to the increase of υ_p contribution and decrease in υ_e contribution.

5.3. The 12GBA tube steel

The low-carbon low-alloy 12GBA steel is widely used in the construction of main oil and gas pipelines. The material was subjected to plastic deformation by rolling to the finite cross-section of bars of 8×8 mm^2 for several passes with step-like temperature decrease from 750 to 550°C [27]. After severe plastic deformation, the steel has a fibrous UFG structure with a lateral fragment size of 0.5 μm. In the longitudinal direction, the length of fragments is 15–20 μm.

The 12GBA tube steel loading was performed by opening of the chevron-notch sides (**Figure 6**).

Figure 13 shows a loading diagram "force P – displacement of notch tips λ" for the 12GBA tube steel. Crack initiation at the tip of the chevron notch is preceded by considerable plastic deformation. A crack initiates at the moment when the load reaches practically reaches a maximum (marked with an arrow). First, the crack slowly grows, and then its propagation
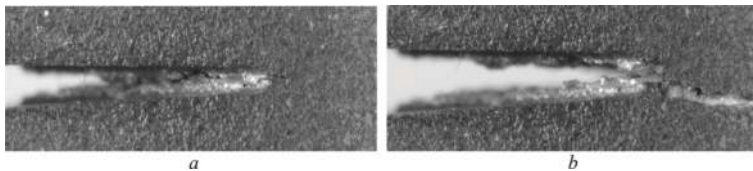

Figure 12. Crack in the chevron-notch zone prior to the fracture (*a*) and the specimen fracture after 4 s (*b*).
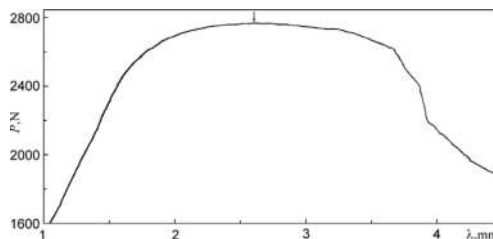

Figure 13. Loading diagram for the 12GBA steel.

Figure 14. Crack propagation in the chevron-notched zone. The 12GBA tube steel in the UFG state.

velocity increases sharply. The calculations by Eq. (5) determine the value of $K_{Ic} = 104$ kJ·m$^{1/2}$ for 12GBA, which is much higher than for the Fe-Ni alloy (75.51 MPa·m$^{1/2}$).

In contrast to the titanium-based alloys, significant processes of plastic deformation are developed in the SMC 12GBA steel in the chevron-notch zone resulting to the extremely viscous fracture behavior. **Figure 14** illustrates the consistent patterns of crack propagation in the chevron-notch zone. From the moment of crack initiation, this process is accompanied by a monotonous drop in the external load (**Figure 13**).

The λ_p/λ_e ratio can serve as a quantitative characteristic of viscosity. For these materials, it differs quite considerably, in particular, at the load peak λ_p/λ_e is 2.6 for 12GBA and λ_p/λ_e is 0.81 for the CC VT6 alloy.

These examples show that at fracture toughness certification of the material, except for SFE, it is important to know the characteristics of λ_p/λ_e and υ_p/υ_e, which determine the effect of plastic deformation on the displacement of load application points and crack opening, respectively. The proposed method allows us to study the fracture toughness of materials without restrictions on the plastic zone size at the crack tip.

6. Conclusion

This chapter presents a new method for determining fracture toughness of materials according to the test data of non-standard small-size chevron-notched specimens. The analytical expressions are obtained being based and derived from the constitutive equations of engineering fracture mechanics to determine the crack-driving force G (specific fracture energy) and the stress intensity factor (SIF) K_{Ic}. Experimental determination of crack length Δl is of principle importance in calculations. During testing, loading diagrams and photographic images of the specimens taken in time intervals are obtained. The displacement of the notch sides, crack opening at the tip of the chevron notch and crack length during its initiation and propagation are measured. This allows us to distinguish the plastic deformation contribution to the displacements that is not related to the change in specimen ductility and therefore does not affect the fracture toughness characteristics of the material.

Due to the fact that change in specimen ductility with increase in the crack length is analytically considered in constitutive relations, the periodic unloading of the specimen applied under standard test conditions of the chevron-notched specimens is excluded in the experiments.

There are no empirical constants and phenomenological dependencies in the calculations. All necessary calculation parameters are determined according to the experimental data. The

method allows us to use the low-power test machines and does not require large amounts of material for the production of specimens, as well as fatigue precracking. The method allows us to certify fracture toughness of the material without restrictions regarding the amount of plastic deformation and in front of the crack tip and in the specimen as a whole. The theoretical analysis has shown that G_c compared to K_{Ic} depends on the Young's modulus E of the material. The higher E is, the lower is G_c under all other conditions being equal. For this reason, the relative values of G_c and K_{Ic} characteristics can differ essentially. Thus, the value of G_c for the Fe-Ni alloy is lower that for the CC VT6 alloy, and the value of K_{Ic} is, on the contrary, higher (**Table 1**).

It is proposed to consider the λ_p/λ_e ratio as an additional fracture toughness characteristic that determines the plastic deformation contribution to the displacement of load application point in relation to the elastic deformation.

Therefore, in order to make fracture toughness certification of the material more complete, it is recommended to determine three fracture toughness characteristics of the material: SIF, SFE and the λ_p/λ_e ratio. According to this method, the fracture toughness characteristics of the VT6, Fe-35.4%Ni alloy and the 12GBA tube steel are determined, which differ in the ability to fracture toughness and the Young's modulus.

Acknowledgements

Author details

Yevgeny Deryugin

Address all correspondence to: dee@ispms.tsc.ru

Institute of Strength Physics and Materials Science of the SB RAS, Tomsk, Russia

References

[1] ASTM Designation E 399-09: Standard Test Method for Linear-Elastic Plane-Strain Fracture Toughness K_{Ic} of Metallic Materials. PA, USA: West Conshohocken; 2009

[2] Methods of Mechanical Testing of Metals. Determination of Fracture Toughness Characteristics under Static Loading. GOST 25.506-85. Moskow: Izdatelstvo standartov; 1985

[3] GOST 4647-80 (ST SEV 1491-79). Moskow: IPK Izdatelstvo standartov; 1998

[4] Ali MB, Abdullah S, Nuawi MZ, Ariffin AK, Nopiah ZM. Evaluating instrumented charpy impact strain signals using curve fitting equations. Journal of Central South University. 2014;**21**:600-609. DOI: 10.1007/s11771-014-1979-3

[5] Miyazaki H, Hyuga H, Yoshizawa YI, Hirao K, Ohji T. Relationship between fracture toughness determined by surface crack in flexure and fracture resistance measured by indentation fracture for silicon nitride ceramics with various microstructures. Ceramics International. 2009;**35**:493-501. DOI: 10.1016/j.ceramint.2008.01.006

[6] Bončina T, Zupanič F, Čekada M, Markoli B. Microindentation of dispersed phases in an Al94Mn 2Be2Cu2 alloy. Journal of Alloys and Compounds. 2010;**505**:486-491. DOI: 10.1016/j.jallcom.2010.06.111

[7] Barker LM. Theory for determining K_{Ic} from small, non-LEFM specimens, supported by experiments on aluminum. International Journal of Fracture. 1979;**16**:515-536. DOI: 10/1007/BF00019921

[8] Wang CT, Pillar RM. Short-rod elastic-plastic fracture toughness test using miniature specimens. Journal of Materials Science. 1989;**24**:2391-2400. DOI: 10.1007/BF01174501

[9] Grant TJ, Weber L, Mortensen A. Plasticity in Chevron-notch fracture toughness testing. Engineering Fracture Mechanics. 2000;**67**:263-276. DOI: 10.1016/S0013-7944(00)00061-8

[10] Soderholm K-J. Review of the fracture toughness approach. Dental Materials. 2010;**26**: e63-e77. DOI: 10.1016/j.dental.2009.11.151

[11] Rakhimkulov RR. Matching of fracture toughness values of K_{1c}, obtained in chevron-notched specimens and based on standard technique for a steel St3sp. Neftegazovoe delo. 2010;**2**:1-10. Available from: http://www.ogbus.ru/authors/Rakhimkulov/Rakhimkulov_1.pdf

[12] Hertzberg RW. Deformation and Fracture Mechanics of Engineering Materials. 3rd ed. New York: Wiley; 1989

[13] Matvienko YG. Models and Criteria of Fracture Mechanics. Moskow: FIZMATLIT; 2006

[14] Timoschenko S, Goodier JN. Theory of Elasticity. New York, Toronto: McGraw-Hill Book Company; 1951

[15] Broek D. Elementary Engineering Fracture Mechanics. Leyden, Netherlands: Noordhoff International Publishing; 1974

[16] Salem JA, Shannon JI Jr, Jenkins MG. Some observations in fracture toughness and fatigue testing with chevron-notched specimens. In: Brown K, Baratta F, editors. Chevron-Notch Fracture Test Experience: Metals and Non-Metals. ASTM STP 1172. Philadelphia: American Society for Testing and Materials; 1992. pp. 9-25

[17] Barker LM. A simplified method for measuring plane strain fracture toughness. Engineering Fracture Mechanics. 1977;**9**:361-369. DOI: 10.1016/0013-7944(77)90028-5

[18] Ruggieri C, Mathias L. Fracture-resistance testing of pipeline girth welds using bend and tensile fracture specimens. Journal of Pipeline Engineering. 2013;**12**:217-227

[19] Roy H, Ray A, Barat K, et al. Structural variations ahead of crack tip during monotonic and cyclic fracture tests of AISI 304LN stainless steel. Materials Science & Engineering, A. 2013;**561**:88-99. DOI: 10.1016/msea.2012.10.074

[20] Bartisch M, Zang ZF, Scheu C, et al. Fracture parameters of chevron-notched Al_2O_3/Nb sandwich specimens. Zeitschrift Fur Metallkunde. 2004;**95**:779-784

[21] Deryugin EE. Improved model of the Griffith crack. Journal of Applied Mechanics and Technical Physics. 1998;**39**:934-942. DOI: 10.1007/BF02468227

[22] Zherebtsov SV et al. Production of submicrocrystalline structure in large scale Ti-6Al-4V billet by warm severe deformation processing. Scripta Materialia. 2004;**51**:1147-1151. DOI: 10.1016/j.scriptamat.2004.08.018

[23] Grigor'ev IS, Meilikhova BZ, editors. Physical Quantities. Handbook. Moscow: Energoatomizdat; 1991

[24] Titanium Alloys. Composition, Structure, Properties. Reference Book. Moscow: VILS-MATI; 2009. 520 p

[25] Deryugin EE, Suvorov BI. Defining the fracture toughness for small-sized samples of materials with submicrostructure. Vestnik SamGU. Technical Sciences. 2012;**36**:123-129

[26] Prokopovich KA. Static fracture toughness of the extraterrestrial Fe-17%Ni alloy. In: Works of XII International Scientific and Technical Ural School-Seminar of Metallographers-Young Metal Science Scientists; Russia. Ekaterinburg: UrFU; 2011. pp. 288-290

[27] Safarov IM, Sergeev SN, Korznikov AV, et al. Fibrous ultrafinegrained structure and properties of rolled low carbon steel 12 GBA. Letters on Materials. 2013;**3**:3-6. DOI: 10.22226/2410-3535-2013-1-3-6